

AIRFOIL SECTIONS FLUCTUATING
PRESSURES AND ROTOR BROADBAND NOISE

F. D'AMBRA
&
A. DAMONGEOT
Société Nationale Industrielle
Aérospatiale
Division Hélicoptères

FIFTH EUROPEAN ROTORCRAFT AND POWERED LIFT AIRCRAFT FORUM
SEPTEMBER 4 - 7 TH 1979 - AMSTERDAM, THE NETHERLANDS

2 Wind tunnel tests

The aim is the measurement of the intensity of pressure variations induced by the turbulent boundary layer on the wall of the airfoil. A Reynolds number of 10^6 was thought sufficient for a full simulation of actual flight conditions ; therefore, low speed subsonic wind tunnel tests (incompressible flow) were carried out on large chord airfoils. Subsequently, the investigation of the compressible range proved necessary.

2.1 Feasibility of measurements

Such measurements can only be carried out if the parasitic sound pressure level generated by the fan in the wind tunnel section is below the level of the aerodynamic pressure fluctuation generated on the airfoil skin by the turbulent boundary layer.

Figure 9 shows that the feasibility of measurements is reached from 250 Hz for a low speed wind tunnel and around 700 Hz for a high speed wind tunnel.

The parasitic noise of the wind tunnel is measured by placing in lieu of the airfoil :

- a B K 1/4" microphone, fitted with a nose cone for the low speed wind tunnel.
- a small lens-shaped profile (22 mm chord) fitted with a KULITE LQ 080 125 S pressure transducer in its center.

2.2 Incompressible flow - S₂ I.A.T. S^t Cyr -

Description of test elements

- 2 NACA 0012 Airfoil sections profiles, with 0.4 and 0.8 m chords respectively mounted "between panels".
- actual airduct cross-section 1.8 m (height) 0.8 m (width).
- 3 wind velocities - 30, 40 and 50 m/s.
- $0.8 \cdot 10^6 \leq \text{Reynolds number} \leq 2.7 \cdot 10^6$;
- angle of attack : $-4^\circ, 0^\circ, 4^\circ, 8^\circ$
- 5 pressure transducers (PITRAN PTM 2) with diameters of 4.75 mm and sensitivities of 1 mV/PASCAL, distributed chordwise over the upper surface at : x/c 0.5, 0.9, 0.925, 0.95, 0.975
- turbulent velocity measurement in the boundary layer with a two-channel TSI hot film anemometer.

Accelerometric measurements made it possible to verify that the vibration level of the profiles during tests was low enough not to affect the signals delivered by the pressure transducers.

Results

It appears that the main pressure fluctuations are concentrated on a small area of the trailing edge ($0.95 < x/c < 1$).

Figure 10 shows the effect of the main parameters upon the skin pressure spectral shape.

- With increasing free stream velocities, the levels rise approximately as V^4
- With an increased incidence or an increased chord, low frequency levels increase to the detriment of high frequency levels with an unvarying point around 2 000 Hz.

1 Introduction

For the last ten years, the noise generated by helicopter rotors has given rise to numerous theoretical and experimental studies.

The imminent implementation of a noise certification standard for helicopters scheduled for January 1st 1980 by ICAO has infused new blood into such studies. Spectra of in-flight helicopter noise measured for the setting-up of this new standard show that a large proportion of the radiated noise is of the broadband type.

This appears on figure 1 showing the spectral analysis of the noise generated by the SA 330 Puma in fly-over configuration from sound levels recorded by a microphone located on the helicopter ground track.

While theoretical studies have been conducted to some depth as regards the rotational noise of rotors (which contribution to the noise spectrum generally lies below 1 000 Hz, i.e. a low frequency range where annoyance units impose only a low penalty), it should be noted that studies made on broadband noise (which contributes in a much larger part to the rotor radiated noise spectrum with penalizing annoyance units) have so far been limited to semi-empirical formulas involving a very limited number of rotor parameters. Figures 2, 3 and 4 briefly state the most widespread semi-empirical formulas. Figure 5 compares theoretical estimate results based on these formulas with measurement results obtained on an SA 330 rotor during a rig rotation test.

This comparison shows among others that the first method does not express very well the variation of levels with respect to frequencies. The second method, semi-empirical, estimates noise levels that are much lower than the measurement results but makes possible a better estimate of the spectral form at high frequencies.

The path followed in this broadband noise study is very close to those adopted for the theoretical estimate of rotational noises, namely :

- Characterization of the emitting source
- Computation of radiated noise using Lighthill noise propagation equations.

The knowledge of source characteristics has been obtained through measurements in a wind tunnel. They were made on a NACA 0012 airfoil in the incompressible and compressible ranges relevant to helicopter rotors and more particularly to their operating aerodynamic conditions near blade tips. A detailed analysis of tests data associated with theoretical and experimental results on the boundary layer characteristics made possible a synthetization of the parietal pressure spectra measured according to the local displacement thickness of the boundary layer. Synthesizing results in this way makes it possible to plot on a single curve the skin pressure spectra of a given profile whatever its chord, Mach number, operating Reynolds number and angle of attack. Also synthesized were the convection speeds and correlation lengths deduced from the measurement processing.

Lowson's formula is used to calculate the noise radiated by the airfoil section originating from these parietal loads considered dipolar. The main characteristics of the radiated noise are analyzed in particular as regards directivity.

The comparison between the calculation results and the experimental results obtained on an SA 330 metal blade rotor during rig rotation tests shows that the theory expresses in a relatively accurate manner the shape of the spectra, the noise levels and the effect of tip speed.

Correlation between 2 pressure transducers

Although the amplitude histogram of the signal delivered by any transducer is characteristic of a gaussian random distribution, it appears on figure 11 that the cross-spectrum phase varies linearly with the frequency. The higher the free speed the weaker the slope. This can be explained by the movement of whirling perturbations within the boundary layer propagating at a speed U_c equal to 0.6 to 0.7 times the free stream velocity.

This phenomenon can also be represented by the $R_{1,2}$ cross-correlation spectrum which varies with the frequency as a damped sine curve. The frequency difference between 2 consecutive maxima is such that the wave length $\lambda = \frac{U_c}{\Delta f}$ corresponds to the distance between the two pressure transducers. Moreover, it is worth noting that $R_{1,2}$, correlation coefficient ($R_{1,2}$ envelope) decreases according to the frequency.

The same characteristics can be found by examining the signals from hot film airspeed sensors located within the boundary layer.

Obviously, skin pressure fluctuations are induced by the speed fluctuations in the turbulent boundary layer.

2.3 S3 CH ONERA compressible flow

Description of test elements

- 1 NACA 0012 profile, with a 0.15 m chord and a 0.45 m span. This profile is half-wing mounted to the wall.
- air duct cross-section : nearly hexagonal ; internal diameter : 0.60 m
- Mach number : 0.15, 0.3, 0.5, 0.6, 0.7, 0.8.
- angle of attack : $0^\circ, \pm 3^\circ, \pm 6^\circ, \pm 8^\circ, \pm 12^\circ$.
- 7 pressure transducers (2 "ELECTRET 20 H.222" and 5 "KULITE LQ 080.125 S")
distributed chordwise at mid-span : upper surface : $x/c = 0.3, 0.5, 0.7, 0.8, 0.9, 1$
lower surface : $x/c = 1$

Results

Figure 12 shows the chordwise distribution of parietal pressure levels. The basic result is that the compressibility effect, beyond $M = 0.5$ for a 1 000 Hz frequency, leads to the distribution of high pressure levels almost over the whole profile surface ; moreover, for $M = 0.8$, the level at 30% from the leading edge is higher by 10 dB than that of trailing edge.

As regards correlations between pressure transducers, the same characteristics as for incompressible airflow are found.

3. Result modelization

3.1 Reduced spectrum

Figure 13 shows all the pressure levels measured by using the $\delta 1$ displacement thickness of the turbulent boundary layer at the relevant measurement points as a reduction parameter.

Two areas of the reduced spectrum can be characterized :

- the reduced low frequency area corresponding to the compressible airflow with a strong decrease of level ($- 8$ dB/octave).
- the reduced high frequency area corresponding to the incompressible airflow with a very low decrease of level (1 to 2 dB/octave).

In such a case, it should be noted that a very close cross-check is obtained from the results given by other authors (SCHLOEMER - Ref. 5).

3.2 Evaluation of the turbulent boundary layer displacement thickness on an airfoil section

As regards the incompressible airflow tests, direct measurements of velocity distribution within the boundary layer have been carried out ; this was no longer possible with a compressible airflow ; therefore, the displacement thickness have been assessed through sophisticated calculation programmes based on GARABEDIAN's and KORNS's methods for potential airflow and on MICHEL's method for boundary layer. With a view to symplifying the analysis of the reduced spectrum in the radiated noise calculations, the boundary layer calculation results for NACA 0012 airfoil section have been redefined (figure 14) ; the following relationship makes it possible to evaluate the effect of the various parameters with good precision :

$$\log \delta 1 = - 3.775 + 1.10 \frac{x}{c} + 0.12 M + 0.8 \log c + 0.0755 \alpha^{\circ}$$

where :

- $\delta 1$: upper surface thickness displacement
- $\frac{x}{c}$: relative abscissa (origin at leading edge)
- M : free stream Mach number
- c : NACA 0012 airfoil chord
- α : angle of attack (degrees).

This formulation is specific to the NACA 0012 airfoil section and can be applied from the laminar/turbulent transition point up to the trailing edge ; for an airfoil section with a smooth surface condition, the abscissa of the transition point can be expressed as a function of the angle of attack by the relationship shown in fig. 15 :

$$X_T/C = - 0.075 \alpha + 0.45$$

other limitations are :

- The Mach number $0.3 \leq M \leq 0.85$
- The moderate angle of attack $- 4^\circ \leq \alpha \leq +6^\circ$ shock cases excepted

3.3 - CORRELATION LENGTH

The evolution of the correlation length l_c , which is defined in Appendix 2, can be expressed by a very simple law in which the only two parameters are the free stream velocity U and the fluctuation frequency f (fig. 16) :

$$l_c = U / f$$

This result is also in correct agreement with SCHLOEMER data(Ref. 5) obtained on flat plates.

4 - RADIATED NOISE CALCULATION MODEL

4.1 - LOWSON FORMULATION

It is considered that the acoustic source region mainly consists of the fluctuating pressure distribution area over the airfoil skin. These pressure fluctuations correspond to force fluctuations over an elemental area. The LOWSON equation (fig. 17. Ref. 3) is thus used under its differential form to calculate the sound pressure radiated by a rotating blade and in the general case of an observer standing in any location of space.

4.2 - MODELIZATION OF THE SOURCE REGION

The characteristics of fluctuating pressure fields measured on stationary airfoils in wind tunnel can be summarized as follows (fig. 18) :

- 1 random pressure fluctuation in any point of the airfoil surface. This property allows each frequency of the source spectrum to be considered individually in the noise propagation equation.

- 2 Between two points taken chordwise within a correlation length, a phase relation exists due to the displacement of Boundary layer vortices at speed $U_c \simeq 0.66 U$. It must be noted that this second property is not incompatible with the first one : it indicates that the LOWSON equation must be split into elemental source regions of which the characteristic dimension is the correlation length ; moreover, for a given frequency, the total radiated sound intensity must be obtained by summing the quadratic means of the partial sound pressures radiated by each elemental source region.
- 3 The distribution of the fluctuating pressure intensity over the source region is defined by the reduced spectrum.

Figure 19 shows the general form of the source function F_p which is mainly the product of a space intensity distribution function and of a space-time fluctuation function ; in addition, the latter includes the effect of the boundary layer vortices displacement.

Figure 20 shows the simplified flow chart of the programme developed for calculating the radiated noise ; the propagation equation is integrated numerically by breaking down the blade area into small elements ΔC chordwise and ΔR spanwise. The emission time is evaluated for each source element by means of an iterative method.

5 - RESULTS

5.1 - GENERAL CHARACTERS OF RADIATED NOISE : DISCRETE FREQUENCY SOURCE

In the case of distribution of a discrete frequency source, the radiated noise signal largely depends on the observer position. Figure 21 shows the acoustic pressure signal resulting from a source distribution at a frequency of 100 Hz (case of an SA 330 rotor blade tip with a 0.537 m chord) :

- When the observer is placed along the rotor shaft axis ($\sigma = 90^\circ$), the acoustic pressure signal is a pure sine wave at the same frequency as that of the source region.
- When the observer moves away from the rotation axis, the received acoustic signal is a complex signal modulated both in amplitude and frequency ; then it shows an impulsive feature all the more pronounced as the observation angle σ with respect to the rotation plane decreases. This complexity is reflected through the general noise calculation programme since each source frequency considered implies a harmonic analysis of the corresponding partial noise signal and the complete spectrum is drawn up step by step by summing the squares of partial Fourier coefficients.

Remark : The presence of cavities or asperities on the tips of rotor blades can in some instances constitute an emergent source of pure tone ; this results in a continuous whistling for an observer standing along the rotor axis and in a noise which is all the more impulsive as the observer moves away from this axis.

Complete spectrum — Effect of radial sections

Figure 22 shows the complete spectrum resulting from the contribution of all source frequencies (uninterrupted line) ; when examined in detail, the shape of this spectrum is not regular ; this is due to the fact that an elemental radial section [itself] shows pronounced lobes which correspond to dominant modes of propagation. The frequency, and particularly the amplitude, of these dominant modes decrease when the radial section being considered comes closer to the hub (effect of decreasing radial velocity Ωr) ; practically, it appears that the emissive section of blades can be limited to 20% of span from the tip ; in fact, figure 22 shows that the contribution of the 1st section (10% from the tip) is at - 2 dB from the total level while the contribution of the 3rd section (10% of relative span centered at $\frac{r}{R} = 0.75$) is at - 8 dB from the total level.

5.2 - COMPARISON BETWEEN THEORY AND EXPERIENCE

Acoustic measurements have been taken on a rotor rig with metal blades fitted on a three-blade hub. The broadband noise calculation method is applied to this rotor for an observer placed along the rotation axis. Figure 23 shows the calculated and measured spectral densities ; it can be noticed that dominant mode lobes actually exist but are not so pronounced as indicated by the calculation ; this effect can be smoothed by introducing radial sections of relative span below 10% in the calculation.

If considering the envelope of calculated points, a very good agreement is obtained between theory and experience as regards :

- absolute noise levels and spectral form,
- effect of rotational speed.

The number and quality of available noise measurements did not allow an accurate study to be made of the effect of pitch and observer position.

6 - FUTURE WORKS

These works will consist in continuing the comparison between theory and experience, especially as regards the effects of noise directivity and blade pitch, and in improving the general calculation method from careful specific measurements made on tail rotor rig in which the effect of rotation speed, pitch, number of blades, observer position will be analyzed.

A simplified calculation method will be developed to allow engineers, not specialized in noise problems to answer quickly to questions raised during the pre-project phase.

Possible means of noise reduction will be investigated ; for example, the effect of an action on the boundary layer can be studied on airfoil sections or rotors in wind tunnel.

7 - CONCLUSIONS

This study shows that the broadband noise generation can be explained, at least for the time being, in a location close to the rotor axis, by considering the skin pressure fluctuations induced by turbulent speeds of the blade boundary layer as acoustic sources.

Despite the number and sometimes the complexity of aerodynamic phenomena involved, a general formulation of the source region characteristics is possible :

- reduced skin pressure spectrum
- boundary layer displacement thickness
- correlation length
- convection speed.

The radiated noise calculation model then developed gives accurate information about absolute levels, spectral form and effect of rotation speed for a rotor of the SA 330 type.

Specific measurements will be taken on other rotors to study the effects of pitch and observer position especially when located within the rotation plane.

Finally, a simplified calculation method will be developed by attempting the introduction of more general aerodynamic parameters.

REFERENCES

- 1 — J.D. SHILLADAY (Mrs) — Helicopter and Convertible rotorcraft noise estimation
WESTLAND HELICOPTERS LIMITED
Research paper N° 387
- 2 — M.R. FINK — Minimum on-axis noise for a propeller or helicopter rotor
AIAA — Vol. 15 — N° 10 — 1978
- 3 — M.V. LOWSON — Theoretical Studies of Compressor Noise
NASA CR 1287 — March 1969
- 4 — J.W. LEVERTON and B.J. SOUTHWOOD — Helicopter Main Rotor Noise :
Do we understand the Mechanisms involved ? GARTEUR 5 Specialist Meeting
on Propeller and Helicopter Rotor noise
PARIS — 1st — 2nd June 1977 — Paper N° 2.2
- 5 — H.H. SCHLOEMER — Effects of pressure gradients on Turbulent — Boundary —
Layer Wall — Pressure Fluctuations
J.A.S.A — 93-113 — Vol. 42 — N° 1-1967
- 6 — R. MICHEL — Couches limites, frottements et transfert de chaleur
Cours à l'E.N.S.A.E.
- 7 — F. BAUER — P. GARABEDIAN — D. KORN — Supercritical wing sections —
Lectures notes in economics and mathematical systems
- 8 — G. VINGUT — Calcul bidimensionnel supercritique avec correction de couche limite
Doc. SNIAS — H/DE.ER 370-64
- 9 — R. LYOTHIER — Ecoulements bidimensionnels transsoniques avec couche limite
autour d'un profil
Doc. SNIAS — H/DE.ER 370-97

ANNEXE 1
DEFINITIONS FOR SIGNAL TREATMENT

2 signals : $P_1(t)$, $P_2(t)$ (Real functions)

FOURIER TRANSFORM : $S(f) = \int_{-\infty}^{+\infty} p(t) e^{-2i\pi f t} dt$
 $S_1(f)$, $S_2(f)$ (Complex function)

AUTO-SPECTRUM

$G_{1.1}(f) = S_1(f) \cdot S_1^*(f)$ (Real function)

$G_{2.2}(f) = S_2(f) \cdot S_2^*(f)$

Where : $S^* = S$ Conjugate (Complex function)

CROSS-SPECTRUM

$G_{1.2}(f) = S_1(f) \cdot S_2^*(f)$ (Complex function)

«CROSS-CORRELATION SPECTRUM» : R 1.2

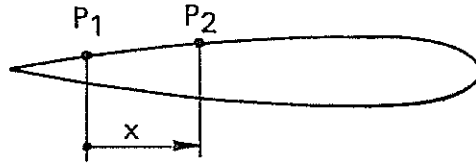
is defined as the real part of the normalized cross-spectrum.

$$R_{1.2} = \text{Real part} \left\{ \frac{G_{1.2}}{\sqrt{G_{1.1} \cdot G_{2.2}}} \right\}$$

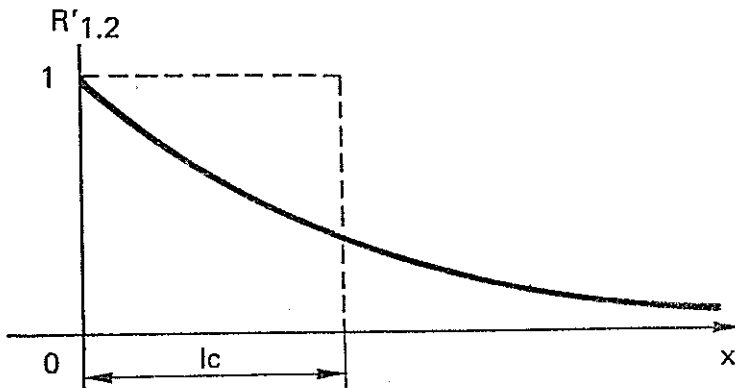
CORRELATION COEFFICIENT

$$R'_{1.2} = \text{Magnitude} \left\{ \frac{G_{1.2}}{\sqrt{G_{1.1} \cdot G_{2.2}}} \right\}$$

ANNEXE 2
CORRELATION LENGTH : l_c



FOR A GIVEN FREQUENCY . f , THE CORRELATION COEFFICIENT $R_{1,2}$ decreases when the distance x between two transducers increases.



$$l_c = \int_0^{\infty} R'_{1,2}(x) dx$$

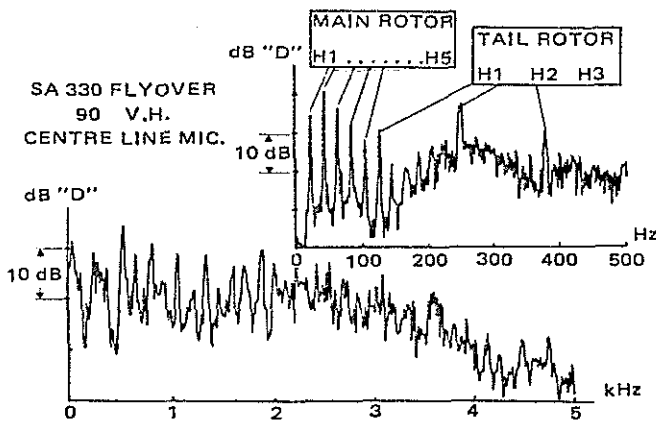


FIG 1 BROAD BAND NOISE CONTRIBUTION IN HELICOPTER NOISE

SA 330 FLYOVER - 90%V.H.
CENTRE LINE MICROPHONE

LEVELS ARE GIVEN IN ANNOYANCE UNIT db "D"

| ROTATIONAL NOISE | | BROADBAND NOISE | GLOBAL |
|------------------|------------|-----------------|--------|
| MAIN ROTOR | TAIL ROTOR | | |
| 83.3 | 82 | 84.4 | 88.1 |

FIG 1a COMPARISON BETWEEN ROTATIONAL AND BROADBAND NOISE CONTRIBUTIONS IN HELICOPTER NOISE

DAVIDSON & HARGEST FORMULA (1)

OASPL AT 500 ft. ALONG THE ROTOR AXIS

$$SPL_{500} = 20 \log T + 20 \log \sqrt{V_T^2 + V_F^2} - 10 \log S - C + C_B$$

- T : THRUST
- V_T : TIP VELOCITY
- V_F : FORWARD VELOCITY
- S : BLADE AREA
- C : CONSTANT TERM (38.7 SI)
- C_B : CORRECTION FACTOR FOR BLADE DESIGN

FIG 2 CURRENT PREDICTION METHOD OF ROTOR BROADBAND NOISE

1/3 OCT. FREQUENCY SPECTRUM

- CENTRE FREQUENCY

$$FS = \frac{0,18 \sqrt{V_T^2 + V_F^2}}{C \sin \alpha + t \cos \alpha}$$

- C : CHORD
 - t : THICKNESS
 - α : BLADE ANGLE OF ATTACK
- } AT 0.9 RADIUS

- * SPECTRUM :

- Symmetrical about center frequency
- Shape following empirical decaying law

FIG 3 CURRENT PREDICTION METHOD OF ROTOR BROADBAND NOISE

FINK FORMULA

$$\underline{OASPL} = 50 \log (V/100) + 10 \log (Sb/R^2) + 10 \log (\cos \phi \cdot \cos \theta/2)^2 + 113,9$$

- V : RELATIVE VELOCITY
- S : BOUNDARY-LAYER THICKNESS AT TRAILING EDGE CALCULATED FOR FLAT-PLATE
 $S = 0,37 C (VC/\nu)^{-0,2}$
- b : SPAN LENGTH
- R : FAR-FIELD DISTANCE
- ϕ : SIDE-LINE ANGLE
- θ : DIRECTION ANGLE RELATIVE TO THE CHORD LINE
- ν : KINEMATIC VISCOSITY

1/3 OCT. SPECTRUM

$$SPL_{1/3} - OASPL = 10 \log \left\{ 0,613 (f/f_{max})^4 \cdot \left[(f/f_{max})^{3/2} \div 0,5 \right]^{-4} \right\}$$

where : $f_{max} = 0,1 V/S$

FIG 4 CURRENT PREDICTION METHOD OF ROTOR BROADBAND NOISE

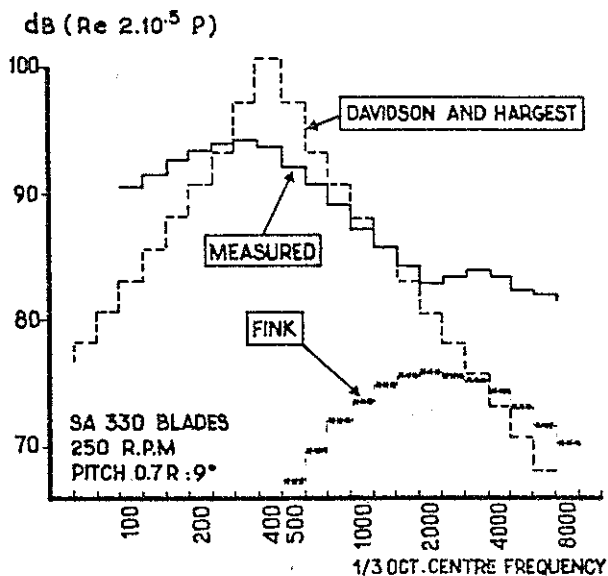


FIG 5 ACCURACY OF CURRENT PREDICTION METHODS

■ SOURCE REGION SURVEY

- WIND TUNNEL MEASUREMENTS ON FIXED AIRFOIL
- * SURFACE PRESSURE SPECTRUM
- PARAMETRIC FORMULATION OF AERODYNAMIC PHENOMENA

■ RADIATED NOISE COMPUTATION MODEL

- * LOWSON'S PROPAGATION EQUATION
- NOISE SOURCES DETAILED REPRESENTATION

■ NOISE RESULTS ANALYSIS

- RADIATED NOISE MAIN CHARACTERISTICS
- THEORETICAL RESULTS/EXPERIMENTAL DATA CORRELATION (WHIRL TESTS ON SA 330 MAIN ROTOR)

FIG 6 ROTOR BROAD BAND NOISE STUDY

INCOMPRESSIBLE FLOW (I.A.T. S2 S^t CYR)

- $0.8 \cdot 10^6 \leq \text{Reyn. } N^r \leq 2.7 \cdot 10^6$
- 2 CHORDS : 0.4 and 0.8 m
- SPEED : 30 to 50 m/s
- * ANGLE OF ATTACK : -4° to $+8^\circ$

MEASUREMENTS

- 5 FLUSH-MOUNTED PRESSURE TRANSDUCERS «PITRAN PTM2»
4 ON THE TRAILING EDGE AREA
1 AT $x/c = 0.5$
- TURBULENT SPEED IN THE BOUNDARY LAYER MEASUREMENTS (HOT FILM ANEMOMETER)

FIG 7 NACA 0012 AERODYNAMIC WIND-TUNNEL TESTS

COMPRESSIBLE FLOW (ONERA. S3 CH)

- CHORD : 0.15 m
- * MACH N^r : $M = 0.15$ to 0.8
- ANGLE OF ATTACK : -12° to 12°

MEASUREMENTS

- * 7 FLUSH-MOUNTED PRESSURE TRANSDUCERS (2 «ELECTRET 20 H 222» - 5 «KULITE LQ 080-125 S»)
 $x/c = 0.30$ to ≈ 1

FIG 8 NACA 0012 AERODYNAMIC WIND-TUNNEL TESTS

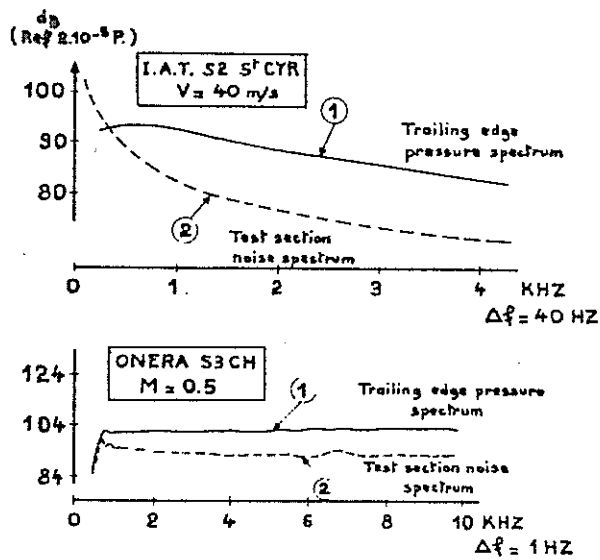


FIG 9 WIND TUNNEL AERODYNAMIC FEASIBILITY TESTS

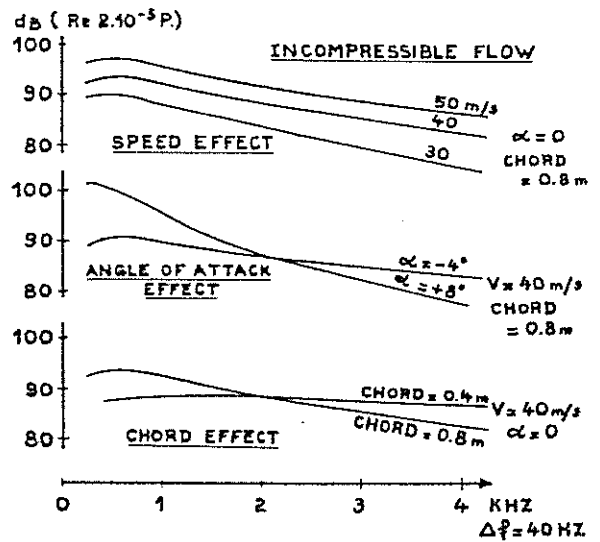


FIG 10 TRAILING EDGE SURFACE PRESSURE SPECTRUM

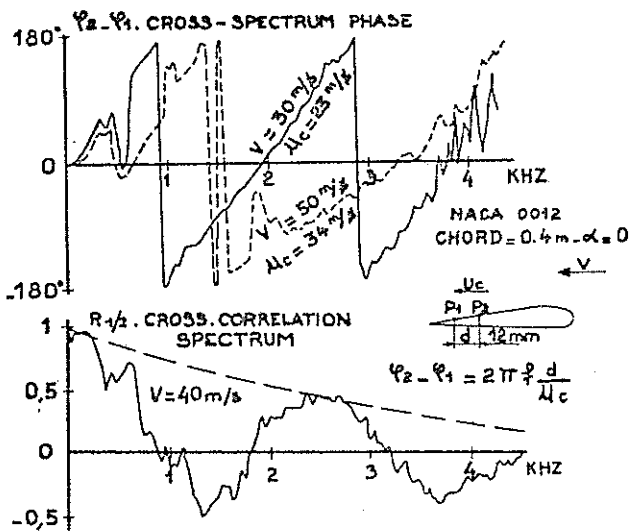


FIG 11 CORRELATION BETWEEN TWO PRESSURE SIGNALS

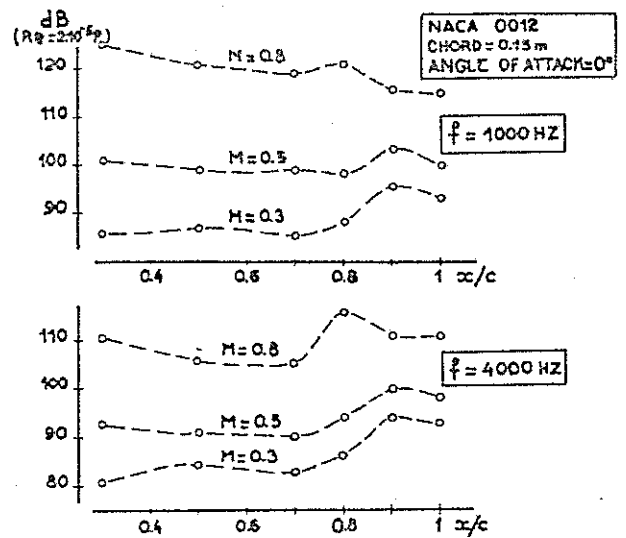


FIG 12 CHORDWISE PRESSURE LEVEL DISTRIBUTION IN COMPRESSIBLE FLOW

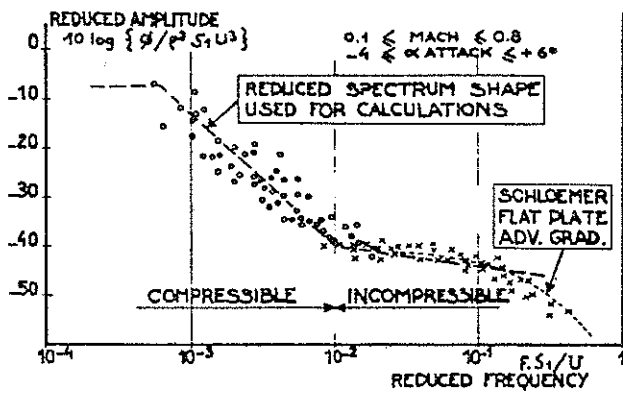
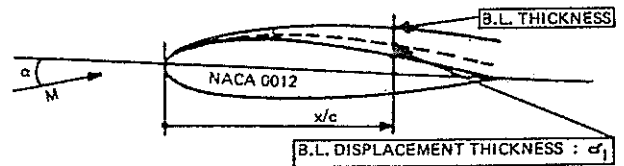


FIG 13 REDUCED FLUCTUATING SURFACE PRESSURE POWER SPECTRUM DENSITY



$$\log \delta_1 = f(x/c, M, C, \alpha, \text{Airfoil})$$

BEST FIT LAW DERIVED FROM THEORETICAL COMPUTATIONS

$$\log \delta_1 = A + B \frac{x}{c} + C.M. + D \log c + E.\alpha^2$$

$$0.3 \leq x/c \leq 1 \quad 0.3 \leq M \leq 0.85$$

$$-4 \leq \alpha^2 \leq +8$$

A, B, C, D, E : CONSTANTS

x : CHORDWISE ABSCISSA

M : FREE STREAM MACH NUMBER

c : CHORD

alpha : ANGLE OF ATTACK

FIG 14 BOUNDARY LAYER DISPLACEMENT THICKNESS EVALUATION

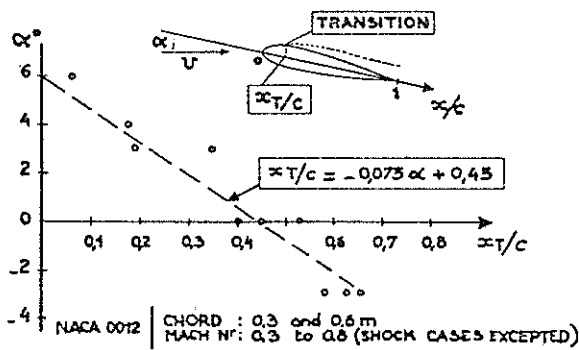


FIG 15 EVOLUTION OF LAMINAR TO TURBULENT TRANSITION REGION

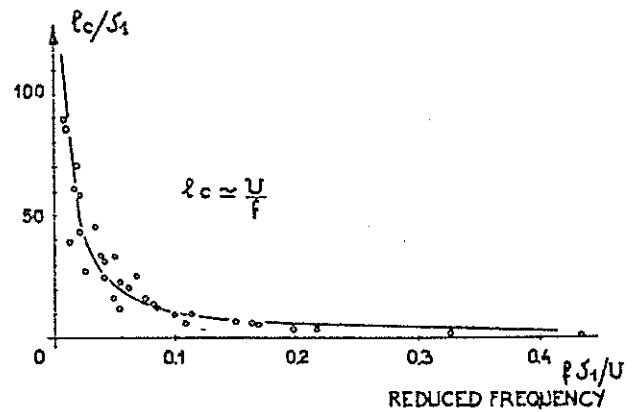


FIG 16 CORRELATION LENGTH

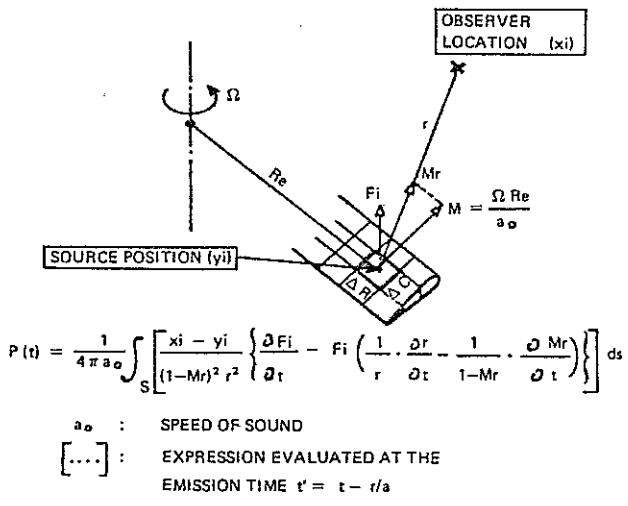


FIG 17 RADIATED ACOUSTIC PRESSURE COMPUTATION — LOWSON FARFIELD EQUATION

- * AT ANY SURFACE POINT :
 — RANDOM PRESSURE FLUCTUATIONS
- * BETWEEN TWO CHORDWISE SURFACE POINTS LOCATED INSIDE A CORRELATION LENGTH :
 — AERODYNAMIC DISTURBANCE TRAVELLING AT $U_c = 0.66 U$

FIG 18 SOURCE MODELIZATION PRINCIPLE

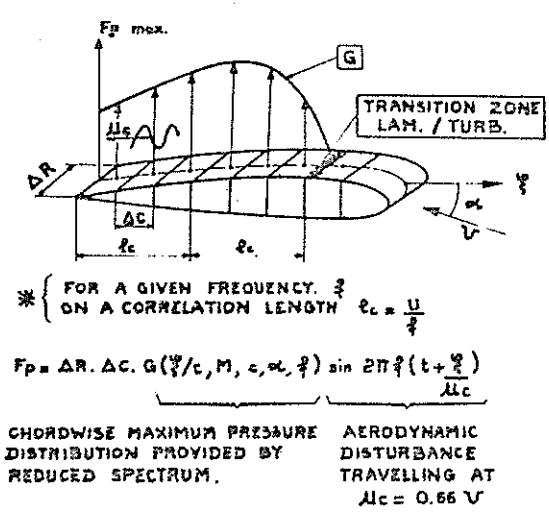


FIG 19 SOURCE REGION MODELIZATION

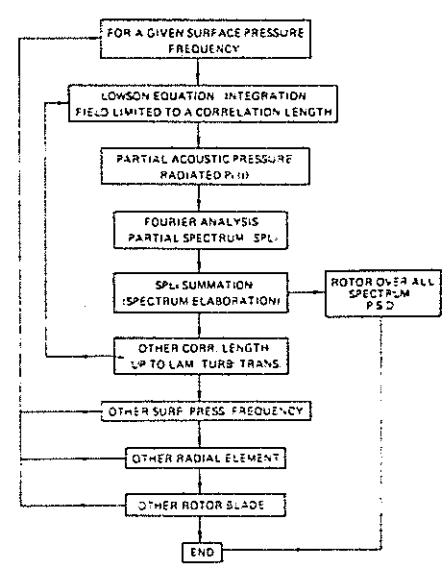


FIG 20 COMPUTATION METHOD PRINCIPLE

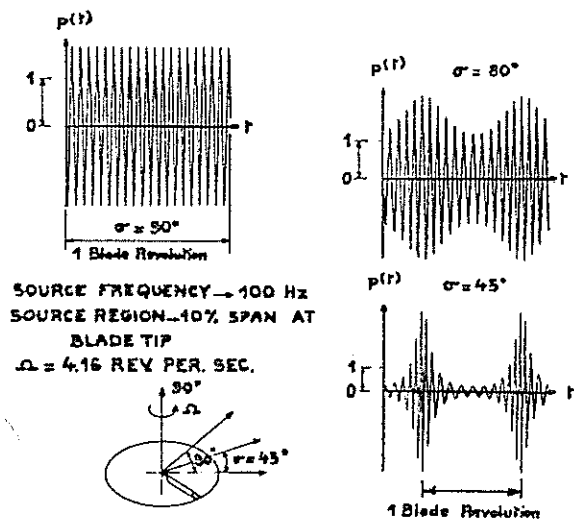


FIG 21 ACOUSTIC PRESSURE SIGNATURE FROM A SINGLE SOURCE FREQUENCY

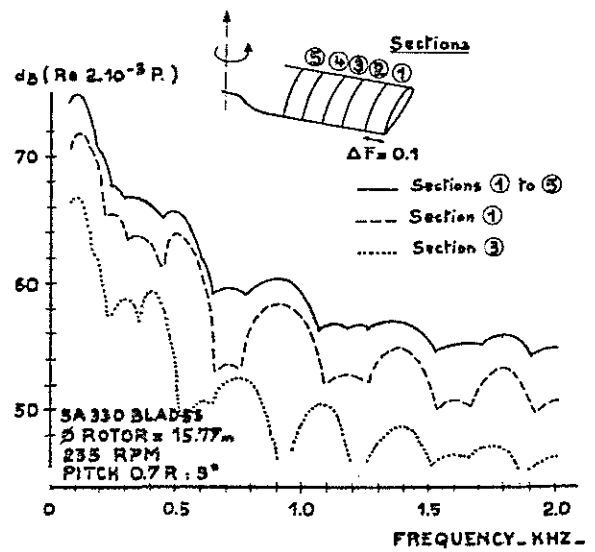


FIG 22 RADIAL BLADE ELEMENTS CONTRIBUTION TO THE TOTAL ROTOR P.S.D.

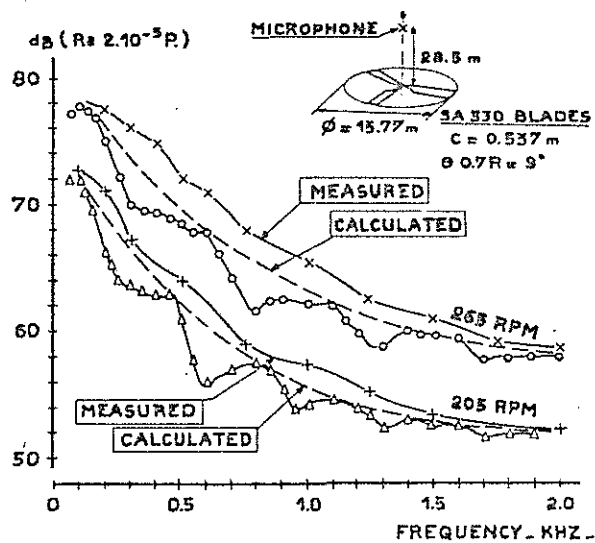


FIG 23 COMPARISON BETWEEN COMPUTED AND MEASURED P.S.D.